KCl, 1% (v/v) horse serum, 2% (v/v) B-27 (Gibco) and a mixture of a penicillin–streptomycin solution (1000 U ml^{-1} and 100 mg ml^{-1}, respectively; Gibco) to a density of 10×10^6 cells ml^{-1} (Gimenez-Cassina *et al.* 2007). High (25 mM)-KCl-containing medium, which is often used for rat cerebellar cultures, was not used in this study because low (5 mM)-KCl-containing medium can improve the long-term viability of mouse cerebellar granule cells, and high-KCl medium maintains the gene expression patterns of granule cells in an immature condition (Mellor *et al.* 1998; Sato *et al.* 2005). A mixture of the cell suspension (20 μl) and the concentrated virus solution (1 μl) was plated onto plastic coverslips (Cell Desk LF1, Sumilon MS-92132; Sumitomo Bakelite, Tokyo, Japan) coated with poly-D-lysine (Sigma-Aldrich) and incubated for 10 h in a CO_2 incubator for virus infection. The DMEM/F12-based medium (700 μl) was added to each dish and replaced by half once a week. Green fluorescent protein fluorescence was first observed at DIV 3, and its expression continued thereafter. In some experiments, ω-agatoxin IVA (0.2 μM; Peptide Institute, Tokyo, Japan), a P/Q-type Ca^{2+} channel blocker, was added to the culture medium every other day from DIV 2 (Mintz & Bean, 1993; Mikuni *et al.* 2013).

Histochemical examination

Cerebellar cultures were fixed in 4% (w/v) formaldehyde in PBS (pH 7.4) for 30 min at room temperature (RT) and incubated overnight at 4°C in PBS containing 0.3% Triton X-100, 0.12% λ-carrageenan, 1% goat serum and 0.02% sodium azide (PBS-XCG) with the following combination of primary antibodies: guinea-pig polyclonal anti-GFP antibody (1:1000 dilution, GFP-GP-Af1180-1; Frontier Institute, Hokkaido, Japan), rabbit polyclonal anti-calbindin D-28K antibody (1:2000 dilution, AB1778; Millipore, Billerica, MA, USA; calbindin is a marker protein of PCs) and mouse monoclonal anti-NeuN antibody (1:2000 dilution, MAB377; Millipore) in PBS-XCG. The samples were further incubated for 3 h at RT in PBS-XCG with the following secondary antibodies: AlexaFluor (AF) 488-conjugated goat anti-guinea-pig IgG antibody (A-11073; Invitrogen), AF 568-conjugated goat anti-rabbit IgG antibody (A-11011; Invitrogen) and AF 680-conjugated goat anti-mouse IgG antibody (A-21058; Invitrogen) in PBS-XCG. All secondary antibodies were used at a concentration of 5 μg ml^{-1}. For examination of nuclear morphology, some cerebellar cultures were stained with Hoechst 33342 (1 μg ml^{-1} in PBS; Dojindo, Kumamoto, Japan) for 15 min at RT after the secondary antibody treatment.

Immunofluorescence was observed under a confocal microscope (A1R; Nikon, Tokyo, Japan) with the following appropriate filter sets: Hoechst 33342 (excitation, 403 nm; emission, 425–475 nm), AF 488 (excitation, 488 nm; emission, 500–550 nm), AF 568 (excitation, 561 nm; emission, 570–620 nm) and AF 680 (excitation, 639 nm; emission, 662–737 nm). Images were obtained with ×10 objective or ×60 water-immersion objective lenses. The confocal pinhole size was 1.0 airy unit. In some experiments, dendrites of PCs were traced from calbindin-positive areas using Neurolucida software (MBF Bioscience, Burlington, VT, USA). The extension of dendritic trees and dendrite complexity were measured by Sholl analysis in Neuroexplorer software (MBF Bioscience; Sholl, 1953; Sawada *et al.* 2010). Concentric spheres were centred on the cell body, and the radii were incremented by 10 μm. The number of branching points within each sphere was counted, and total dendritic length was measured. The cell densities of PCs and granule cells were calculated in each culture by averaging four values of cell density measured from a single image obtained around the centre of the culture with a ×10 objective lens. These measurements were performed using NIS-Elements AR 3.2 software (Nikon).

Data are provided as the means ± SD, and n is the number of experiments. Statistical significance was tested using the Mann–Whitney U test unless otherwise stated (significance, $P < 0.05$). GraphPad Prism 5 (GraphPad Software, San Diego, CA, USA) and StatView 5 software (SAS Institute, Cary, NC, USA) were used for the analysis. In Figs 2–4 and 6–8 and Tables 1 and 2, statistical analysis was performed between cells expressing the R424H mutant and those expressing GFP alone or between cells expressing the R424H mutant and those expressing WT mKv3.3.

Expressions of heterologous proteins in *Xenopus* oocytes

The detailed procedures have been described previously (Kubo & Murata, 2001). Briefly, linearized WT or R424H mutant cDNA in pcDNA3 was used as a template to produce capped cRNA using T7 RNA polymerase (mMESSAGE mMACHINE; Ambion, Austin, TX, USA). *Xenopus* oocytes were collected from frogs anaesthetized in water containing 0.15% (w/v) tricaine. The isolated oocytes were treated with collagenase (2 mg ml^{-1}; type 1; Sigma-Aldrich) and injected with 50 nl of nuclease-free water containing 10 ng of WT *mKv3.3* cRNA, a mixture of 10 ng of WT and 10 ng of R424H mutant cRNAs, or 10 ng of R424H mutant cRNA. The oocytes were then incubated at 17°C in frog Ringer solution containing (mM): 88 NaCl, 1 KCl, 2.4 $NaHCO_3$, 0.3 $Ca(NO_3)_2$, 0.41 $CaCl_2$ and 0.82 $MgSO_4$, pH 7.6, with 0.1% (v/v) penicillin–streptomycin solution (Sigma-Aldrich) for 2–3 days before recordings.

Electrophysiological recording from *Xenopus* oocytes

Potassium currents were recorded under a two-electrode voltage clamp using an OC-725C amplifier (Warner Instruments, Hamden, CT, USA) and Clampex 10.3 software (Molecular Devices, Sunnyvale, CA, USA). The signals were digitized at 10 kHz using a Digidata 1322A (Molecular Devices). The microelectrodes were filled with an electrode solution containing 3 M potassium acetate and 10 mM KCl. The oocytes were perfused with a bath solution containing (mM): 96 NaCl, 2 KCl, 1.8 $CaCl_2$, 1 $MgCl_2$ and 5 Hepes (pH adjusted to 7.2 with NaOH). All experiments were performed at 25°C. The data were analysed using Clampfit 10.3 software (Molecular Devices) and Igor Pro 6 software (Wavemetrics, Lake Oswego, OR, USA) with the added import functionality provided by the ReadPclamp XOP of the NeuroMatic software package (http://www.neuromatic.thinkrandom.com/). To calculate conductance–voltage relationships, outward currents were activated by applying 1000 ms voltage steps from a holding potential of −80 mV to potentials up to +70 mV in 10 mV increments. The equilibrium potential of K^+ ($E_K = -104.0$ mV) was calculated from the intracellular concentration of K^+ (109.5 mM) in the *Xenopus* oocyte (Costa *et al.* 1989). To determine steady-state inactivation, cells were held at −80 mV before applying a 1000 ms prepulse to potentials between −80 and +60 mV in 10 mV increments, followed by a 250 ms test pulse to +20 mV. Steady-state inactivation (I/I_{max}) curves were fitted with the Boltzmann function, $I/I_{max} = 1/[1 + \exp(V - V_{\frac{1}{2}})/k]$, where k is a slope factor. To measure the rates of deactivation, outward currents were evoked by stepping from a holding potential of −80 mV to +50 mV for 5 ms and then stepping to potentials between −60 and +10 mV in 10 mV increments for 50 ms. The time constant of recovery (τ_{recove}) from inactivation was determined by depolarizing the cells to +50 mV for 1000 ms from a holding potential of −80 mV. A step to −80 mV of variable duration was followed with test pulses to +50 mV for 200 ms in 500 ms increments. The data points were fitted with a single exponential function. The time constants of inactivation (τ_{inacti}) and deactivation were obtained by fitting current traces with a single exponential function on the inactivating and deactivating phases of the traces, respectively.

Whole-cell patch-clamp recordings from cultured PCs

In most recordings, cerebellar cultures were constantly perfused (2 ml min^{-1}) with oxygenated artificial cerebrospinal fluid (ACSF) containing (mM): 120 NaCl, 2.5 KCl, 2 $CaCl_2$, 1 $MgCl_2$, 26 $NaHCO_3$, 1.25 NaH_2PO_4, 17 D-glucose and 0.1 picrotoxin (Tocris Bioscience, Bristol, UK; a $GABA_A$ receptor antagonist), bubbled with 5% CO_2–95% O_2 at 26°C. The other recordings were performed in Hepes-buffered ACSF containing (mM): 140 NaCl, 2.5 KCl, 2 $CaCl_2$, 1 $MgCl_2$, 10 D-glucose and 10 Hepes (pH adjusted to 7.4 with NaOH), bubbled with 100% O_2. Outward currents were recorded in Hepes-buffered ACSF containing (mM): 0.2 $CdCl_2$, 0.1 picrotoxin, 0.05 6,7-dinitroquinoxaline-2,3-dione (DNQX; Tocris Bioscience; a AMPA/kainate receptor antagonist,) and 0.001 TTX (Wako Pure Chemical Industries). Hepes buffer was used to avoid the precipitation of $CdCO_3$.

Cells were visualized on the stage of an upright microscope (BX50WI; Olympus, Tokyo, Japan) using a ×40 water-immersion objective lens with Nomarski optics and a near-infrared CCD camera (C-3077-79; Hamamatsu Photonics, Hamamatsu, Japan). Green fluorescent protein-positive cells were visualized and selected using epifluorescence optics (Olympus). Patch pipettes were made from borosilicate glass capillaries to reduce pipette capacitance (GC150F-100; Harvard Apparatus, Holliston, MA, USA) and had a resistance of 1.5–2.5 MΩ when filled with a potassium gluconate-based internal solution containing (mM): 145 potassium gluconate, 5 KCl, 0.1 EGTA, 5 Mg-ATP, 5 disodium phosphocreatine, 0.3 Na_2-GTP, 10 Hepes–KOH and 10 biocytin (Sigma-Aldrich), pH 7.3. The liquid junction potential (−10 mV) was corrected offline. Whole-cell patch-clamp recordings were conducted in GFP-positive PCs at DIV 8–10. Purkinje cells were identifiable by their large somatic size (Tabata *et al.* 2000), and their identity was confirmed by intracellular staining with biocytin. Patch-clamp recordings were acquired using a Multiclamp 700B amplifier with Clampex 10.3 software (Molecular Devices). Signals were filtered at 6–10 kHz and digitized at 10–50 kHz using a Digidata 1440A (Molecular Devices). In voltage-clamp conditions, series resistance was compensated electronically by 80–90%, and in current-clamp conditions, it was performed using the bridge balance and capacitance neutralization. Outward currents were activated with 500 ms voltage steps from −70 mV to voltages ranging from −60 to +40 mV in 10 mV increments. Leak currents were subtracted online by the *P*/4 protocol (Armstrong & Bezanilla, 1974). The recorded currents were normalized to cell capacitance, which was calculated from the transient current evoked by applying a small voltage step (−5 mV, 20 ms duration) from a holding potential of −70 mV in voltage-clamp conditions. Spontaneous excitatory post-synaptic currents (sEPSCs) were recorded at a holding potential of −80 mV for 250 s in the presence of picrotoxin and detected offline using the template search function in the Clampfit 10.3 software. Action potentials were evoked by depolarizing current pulses in current-clamp conditions (10 ms duration, from 0 to 200 pA in 10 pA increments; or 200 ms duration, from 0 to 200 pA in 20 pA increments). The resting membrane potentials were

adjusted to −60 mV by current injection. Spontaneous firing was recorded at resting membrane potential for 300 s. The half-amplitude width of the action potential was measured at the mid-point between the threshold and peak. Action potential amplitude was measured between the threshold and peak.

Fluorescence imaging of calcium

To monitor the free $[Ca^{2+}]_i$ of PCs, cerebellar cultures at DIV 8–10 were incubated with Hepes-buffered ACSF containing fura-2 AM (0.01 mM; Invitrogen) for 1 h at 37°C. The cells were visualized and perfused with Hepes-buffered ACSF at the same settings as those used for the patch-clamp recordings. For fura-2 excitation, the cultures were illuminated alternately at 340 and 380 nm wavelengths using a 100 W xenon lamp source, a fura-2 filter set (ET FURA2; Chroma Technology, Brattleboro, VT, USA), and a filter wheel (Ludl Electronic Products, Hawthorne, NY, USA). The fluorescence was filtered through a bandpass filter (470–550 nm) and captured using an EMCCD camera (iXon3 DU897; Andor Technology, Belfast, UK). The experiments were controlled by Andor iQ software (Andor Technology). The regions of interest were defined as the shape of the GFP-expressing Purkinje cell bodies. The $[Ca^{2+}]_i$ was calculated according to the previously described method with a dissociation constant of 224 nM (Grynkiewicz *et al.* 1985). The maximal and minimal fluorescence ratios (R_{max} and R_{min}) were measured after addition of the calibration solutions. The R_{max} was measured in Hepes-buffered ACSF containing 5 μM ionomycin (Sigma-Aldrich), and R_{min} in Hepes-buffered, Ca^{2+}-free ACSF containing 10 mM EGTA and 5 μM ionomycin. In some experiments, the cultures were perfused for 5 min with high-K^+ ACSF, in which 12.5 mM NaCl was replaced by equimolar KCl (total $[K^+]$, 15 mM) to elevate $[Ca^{2+}]_i$. Basal $[Ca^{2+}]_i$ was obtained as an average for a 7 min period from the beginning of the recordings, and elevated $[Ca^{2+}]_i$ for a 5 min period during high-K^+ ACSF perfusion.

Results

R424H mutant subunits exhibit a dominant-negative effect against WT mKv3.3 subunits without affecting WT subunit expression in heterologous expression systems

We examined whether the biophysical properties of hKv3.3 with the R423H mutation were conserved in mKv3.3 with the R424H mutation using the *Xenopus* oocyte expression system and two-electrode voltage-clamp recording (Figueroa *et al.* 2010; Minassian *et al.* 2012). In WT mKv3.3-expressing oocytes, depolarizing voltage steps from a holding potential of −80 mV evoked outward currents that became more apparent when the membrane was depolarized to potentials more positive than −10 mV (Supplemental Fig. S2*Aa* and S2*C*; a $V_{1/2}$ of activation of 25.5 ± 3.1 mV, $n = 19$), and the currents showed inactivation (Supplemental Fig. S2*Aa*, $n = 11$) and fast deactivation (deactivation $\tau = 0.948 \pm 0.15$ ms at −40 mV, $n = 11$; trace not shown). These results well reflected the reported properties of Kv3.3 channels, i.e. fast activation, positively shifted voltage dependence, N-type inactivation and a fast deactivation rate (Rae & Shepard, 2000; Rudy & McBain, 2001; Desai *et al.* 2008). In R424H mutant-expressing oocytes, negligible currents were observed at potentials more positive than +20 mV (Supplemental Fig. S2*Ac* and S2*B*), and the peak amplitudes were not significantly larger than those recorded in water-injected oocytes (Supplemental Fig. S2*B*; not significant by Student's unpaired *t* test), indicating that most of the currents were derived from endogenous channels present in *Xenopus* oocytes. When cRNA of WT and R424H mutant mKv3.3 was injected at a 1:1 ratio (WT+R424H), the $V_{1/2}$ of activation was significantly left-shifted, by 9.05 mV, compared with oocytes expressing WT subunits alone (Supplemental Fig. S2*C*; WT+R424H, 15.6 ± 9.2 mV, $n = 21$; WT, 24.6 ± 6.1 mV, $n = 19$; $P < 0.001$ by Student's unpaired *t* test). The value of k was decreased by 4.29 mV (WT + R424H, $k = 9.82 \pm 2.4$ mV, $n = 21$; WT, $k = 14.1 \pm 3.1$ mV, $n = 19$; $P < 0.001$ by Student's unpaired *t* test), and the time constant of activation (τ_{acti}) at +40 mV was 2.03-fold slower (Supplemental Fig. S2*Da* and S2*Db*; $P < 0.001$ by Student's unpaired *t* test). These results are consistent with previous reports of hKv3.3 with R423H mutation (Figueroa *et al.* 2010; Minassian *et al.* 2012) and indicate that the functional effects of this mutation are well conserved between humans and mice.

Coexpression of R424H mutant and WT subunits accelerates the inactivation kinetics and slows the recovery from inactivation compared with WT subunits alone

In order to reveal further the unknown biophysical properties of hKv3.3 with the R423H mutation, we investigated the inactivation kinetics, steady-state inactivation and recovery from inactivation of WT+R424H mutant channels. The τ_{inacti} of WT+R424H mutant channels was more than 2-fold faster than that of channels composed of WT subunits alone in the range of +10 to +70 mV depolarizing steps (Fig. 1*A*), and the $V_{1/2}$ of inactivation was significantly left-shifted, by 9.67 mV, compared with that of WT subunits (Fig. 1*B*; WT+R424H, $V_{1/2} = -4.39 \pm 7.09$ mV, $n = 12$; WT, $V_{1/2} = 5.28 \pm 5.33$ mV, $n = 11$; $P < 0.01$ by

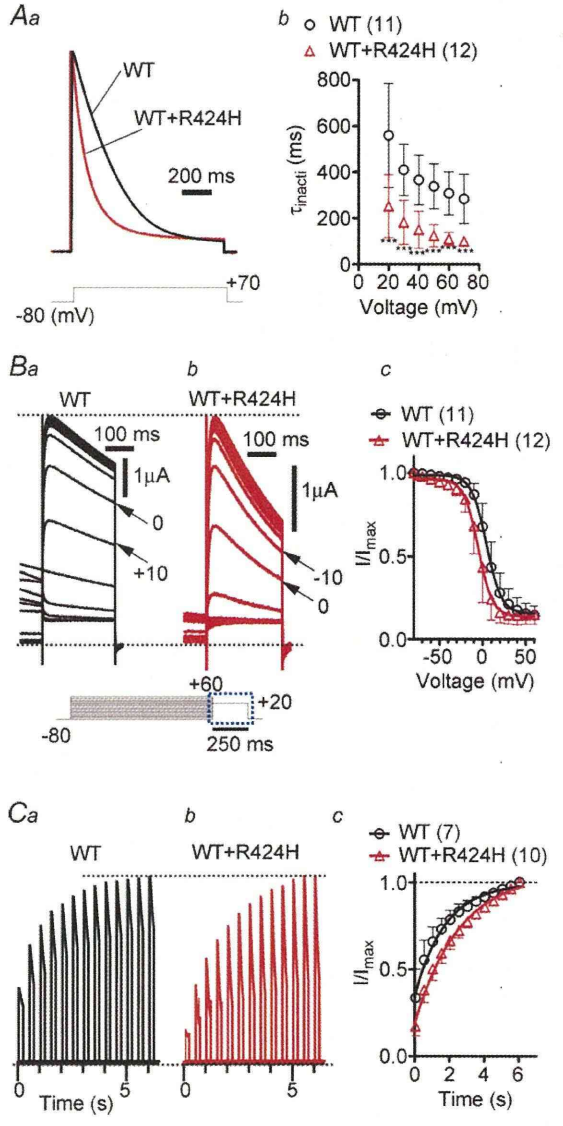

Figure 1. Coexpression of R424H mutant and wild-type (WT) subunits in *Xenopus* oocytes accelerates the inactivation kinetics and slows the recovery from inactivation compared with WT subunits alone

Aa, representative traces evoked by stepping from a −80 mV holding potential to +70 mV. The current traces are scaled to the same peak amplitude. *Ab*, the plots of the inactivation time constant (τ_{inacti}) were determined by fitting the falling phases of currents obtained in Supplemental Fig. S2*A* with a single exponential function. *Ba* and *b*, comparison of steady-state inactivation, which was obtained by changing the membrane potential from a prepulse potential ranging from −80 to +60 mV in 10 mV increments to a test voltage step of +20 mV to record tail currents. *Ba* and *b* shows traces of tail currents, and their corresponding voltage pulses are given under the traces surrounded by the dotted rectangle. *Bc*, the tail current amplitudes were normalized to the maximal current, and the resulting plots were fitted with the Boltzmann function, $I/I_{max} = 1/[1 + \exp(V - V_{1/2})/k]$, where k is a slope factor. *C*, recovery from inactivation in WT channels and WT+R424H mutant channels. *Ca* and *b*, the recovery time constant (τ_{recove}) was determined by depolarizing the cells to +50 mV for 1000 ms from a holding potential of −80 mV. A step to −80 mV of variable duration was followed with test pulses to +50 mV for 200 ms in 500 ms increments. *Cc*, time course of the recovery from inactivation. The curves were fitted with a single exponential function to obtain τ_{recove}. Here and in the following figures, error bars indicate standard deviation, the numbers in parentheses indicate the number of experiments, and statistical significance was tested using Mann-Whitney's *U* test unless otherwise stated (significance, $P < 0.05$). ***$P < 0.001$.

Student's unpaired *t* test). The τ_{recove} from inactivation of WT+R424H was significantly slower than that of WT (Fig. 1*C*; WT+R424H, $\tau_{recove} = 2.62 \pm 0.60$, $n = 10$; WT, $\tau_{recove} = 1.78 \pm 0.08$, $n = 7$; $P < 0.01$ by Student's unpaired *t* test). These results indicate that coexpression of WT and R424H mutant subunits accelerated the inactivation kinetics and slowed recovery from inactivation.

Expression of R424H mutant subunits in cerebellar cultures induces PC death and impairs dendritic development

Spinocerebellar ataxia type 13 patients show cerebellar symptoms and cerebellar atrophy, suggesting shrinkage of the cerebellar cortex and degeneration of cerebellar neurons (Waters *et al.* 2006; Figueroa *et al.* 2010, 2011). In order to explore the effects of the R424H mutant on cell survival, dendritic development and electrophysiological properties in cerebellar neurons, mouse cerebellar cultures were infected at DIV 0 with lentiviruses expressing WT or R424H mutant subunits together with GFP. Given that SCA13 is an autosomal dominant disorder and Kv3 channels are formed by the assembly of four pore-forming subunits, hKv3.3 channels in SCA13 patients are considered to be heteromultimer channels consisting of WT and mutant subunits (MacKinnon, 1991; Figueroa *et al.* 2010; Minassian *et al.* 2012). When R424H mutant subunits were lentivirally expressed in cultured PCs, the subunits were expected to incorporate into endogenous mKv3.3 channels, mimicking the pathological condition.

Green fluorescent protein fluorescence was observed after DIV 3, and >90% of PCs were GFP positive (Fig. 2*A–C*). In the immunohistochemical experiments, PCs were immunostained with anti-calbindin antibody and granule cells with anti-NeuN antibody. Mullen *et al.* (1992) reported that PCs are not stained with anti-NeuN antibody *in vivo*. In agreement with their report, PCs and GABAergic interneurons were NeuN negative in our culture conditions (Supplemental Fig. S3*A* and S3*B*). The mKv3.3 protein in WT-expressing PCs at DIV 10 was significantly overexpressed (by 8.3-fold) compared with that in PCs expressing GFP alone (Supplemental Fig. S3*E*). In contrast to the clear expression of mKv3.3 protein

in PCs (Goldman-Wohl *et al.* 1994), mKv3.3 expression was not detected in cultured granule cells (Supplemental Fig. S3*C*), differing from a previous report using an *in vivo* preparation (Chang *et al.* 2007). Consistent with a previous report (Tabata *et al.* 2000), the relative densities of GFP- and WT-expressing PCs decreased in a day-dependent manner (Fig. 2*A*, *B* and *D*). Until DIV 7, the relative densities of PCs did not differ significantly between R424H mutant-expressing and control cultures (Fig. 2*Aa*, *Ba*, *Ca* and *D*; $P = 0.346$ between GFP and R424H; $P = 0.222$ between WT and R424H). At DIV 11, however, the density of PCs in R424H mutant-expressing cultures was significantly decreased (Fig. 2*Ab*, *Bb*, *Cb* and *D*; $P < 0.01$ between GFP and R424H; $P < 0.01$ between WT and R424H). At DIV 14, ~40% of PCs still survived in GFP- or WT-expressing cultures (Fig. 2*Ac*, *Bc*, *Cc* and *D*), whereas there were few surviving PCs in R424H mutant-expressing cultures. Relative cell densities and the percentage of GFP-positive cells of granule cells at DIV 14 were also quantified, but there were no significant differences between R424H mutant-expressing and control cultures (Fig. 2*Ac′*, *Bc′*, *Cc′* and *E*; cell densities, $P = 0.0952$ between GFP and R424H; $P = 0.117$ between WT and R424H; and percentage of GFP-positive cells, GFP, 65.9 ± 8.3%, $n = 5$; WT, 64.0 ± 7.4%, $n = 5$; R424H, 59.8 ± 8.1%, $n = 5$; $P = 0.421$ between GFP and R424H; $P = 0.310$ between WT and R424H), indicating that expression of R424H mutant subunits did

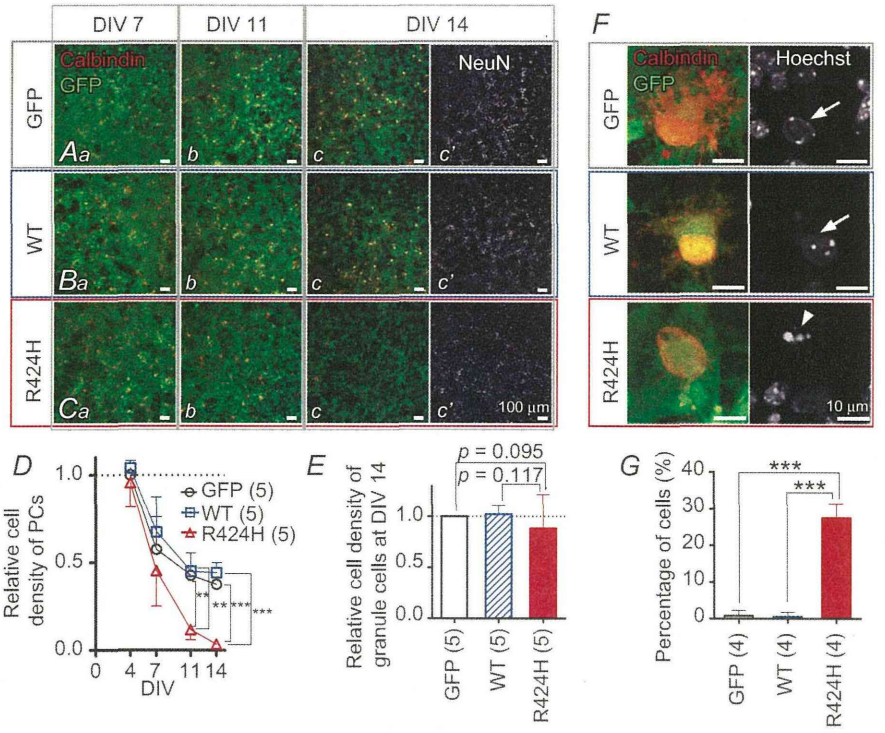

Figure 2. Lentivirus-mediated expression of R424H mutant subunits in cerebellar cultures decreases the density of Purkinje cells (PCs) but not of granule cells

A–C, immunofluorescence images of cerebellar cultures infected with lentiviral vectors expressing green fluorescent protein (GFP) alone (*Aa–c*), WT subunits and GFP (*Ba–c*) or R424H mutant subunits and GFP (*Ca–c*; see Methods). Green fluorescent protein fluorescence was enhanced by immunostaining with guinea-pig anti-GFP antibody and AlexaFluor (AF) 488-conjugated goat anti-guinea-pig antibody. Purkinje cells were visualized by immunolabelling with rabbit anti-calbindin antibody (red signals in *A–C*). *Ac′*, *Bc′* and *Cc′*, granule cells were selectively immunolabelled with mouse anti-NeuN mouse antibody (see Supplemental Fig. S3*A* and *B*). *D*, relative cell density of PCs plotted as a function of days *in vitro* (DIV). The density was normalized to the value of PCs expressing GFP alone at DIV 4. *E*, relative cell density of granule cells at DIV 14. The density was normalized to the mean cell density of granule cells in cultures lentivirally expressing GFP alone at DIV 14. *F* and *G*, R424H mutant-expressing PCs exhibiting chromatin condensation. *F*, representative fluorescence images of PCs at DIV 8. For nucleus detection, the PCs were stained with Hoechst 33342. Normal nuclei of PCs are indicated by arrows (GFP and WT), whereas a nucleus exhibiting chromatin condensation is marked with an arrowhead (R424H). *G*, summary of the percentages of PCs with chromatin condensation at DIV 8. The statistical analysis was conducted using Student's unpaired *t* tests. In the following figures and tables, the statistical analysis was conducted between cells expressing the R424H mutant and those expressing GFP or between cells expressing R424H mutant and those expressing WT subunits. $^{**}P < 0.01$ and $^{***}P < 0.001$.

not affect the survival of granule cells. The difference in cell survival between PCs and granule cells may be because cultured granule cells do not express endogenous mKv3.3 protein (Supplemental Fig. S3*C*), and R424H mutant subunits were thus unable to form multimeric channels with the endogenous mKv3.3 subunits in the cells (see Discussion). These results indicate that R424H mutant subunits induced PC death and worsened their survival in a day-dependent manner.

To examine the cell death-induced morphological defects in the nuclei of PCs, cerebellar cultures expressing GFP alone, WT mKv3.3 or the R424H mutant were stained with Hoechst 33342 at DIV 8 (Fig. 2*F*). Chromatin in nuclei of GFP- or WT-expressing PCs was stained moderately, with some small bright granules (Fig. 2*F*, arrows in GFP and WT panels), demonstrating normal nuclear morphology. In contrast, PCs expressing R424H mutant subunits showed clear chromatin condensation (Fig. 2*F*, arrowhead in R424H panel). The percentages of PCs exhibiting this chromatin condensation were significantly different between R424H mutant-expressing PCs and the control group (Fig. 2*G*; $P < 0.001$ by Student's unpaired *t* test). These results suggest that the expression of R424H mutant subunits might induce apoptotic cell death in PCs.

At DIV 7, several neurites were observed in GFP- and WT-expressing PCs, which had morphologies similar to those of R424H mutant-expressing PCs at this stage (Fig. 3*Aa′*, *Ba′* and *Ca′*). However, at DIV 11, GFP- and WT-expressing PCs had elongated immature dendrites, whereas R424H mutant-expressing PCs did not show dendritic extension (Fig. 3*Ab′*, *Bb′* and *Cb′*). Sholl analyses of the dendritic arbors revealed that the number of dendritic intersections in R424H mutant-expressing PCs was significantly smaller than that in GFP-expressing (Fig. 3*D*, at distances of 10–50 μm from the cell body; $P < 0.01$) or WT-expressing PCs (Fig. 3*D*, at distances of 10–40 μm; $P < 0.01$). These results clearly demonstrate that in addition to the induction of cell death, expression of R424H mutant subunits in PCs decreases the survival rate and impairs dendritic development.

R424H mutant-expressing PCs exhibit lower outward current density

The results using *Xenopus* oocytes showed that expression of R424H mutant subunits significantly modulated WT mKv3.3 channel function (Fig. 1 and Supplemental Fig. S2). Thus, similar effects would be predicted in PCs lentivirally expressing R424H mutant subunits. In order to determine how these electrophysiological properties were affected, whole-cell patch-clamp recordings were performed using cultured PCs expressing GFP only, WT subunits or R424H mutant subunits at DIV 8–10.

Purkinje cells could be identified by their large cell bodies (cell body diameters of PCs at DIV 10, 17.2 ± 2.6 μm, $n = 78$; those of other neurons, 7.26 ± 1.7 μm, $n = 226$), and the recordings were confirmed by a combination of intracellular staining and immunocytochemical staining (Supplemental Fig. S4*A*). The cell capacitance of R424H mutant-expressing PCs was significantly lower than that of GFP- or WT-expressing PCs (Table 1; $P < 0.001$ in R424H *versus* GFP and in R424H *versus* WT), reflecting the impairment of dendritic development (Fig. 3*D*). However, the resting membrane potential and input resistance of R424H mutant-expressing PCs showed no difference when

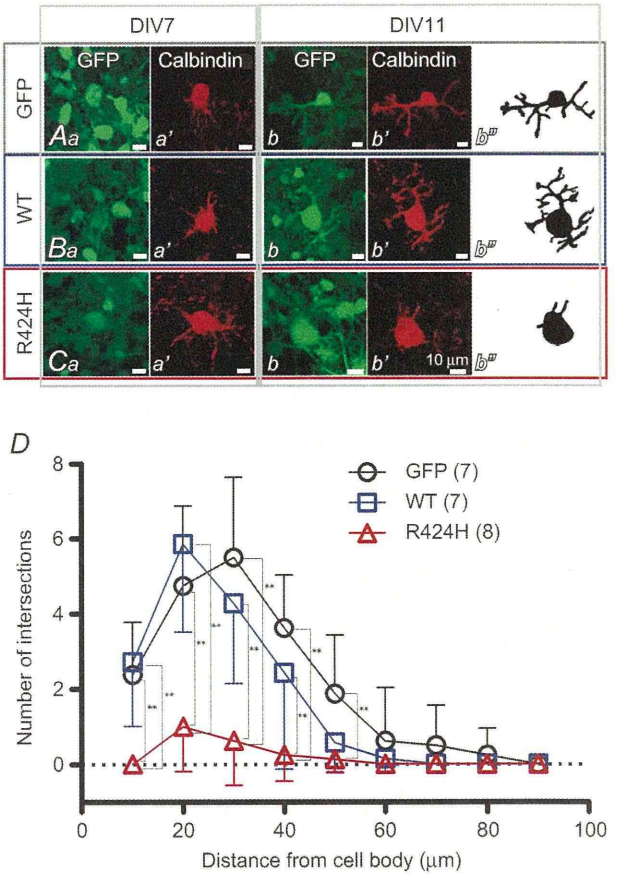

Figure 3. R424H mutant-expressing PCs exhibit impaired dendritic development
A–C, immunofluorescence images of PCs expressing GFP alone (*Aa–b′*), WT subunits and GFP (*Ba–b′*) and R424H mutant subunits and GFP (*Ca–b′*). *Ab″*, *Bb″* and *Cb″*, morphology of PCs expressing GFP (*Ab″*), WT subunits and GFP (*Bb″*) and R424H mutant subunits and GFP (*Cb″*) are depicted for clarity. Each PC was traced using Neurolucida software. *D*, summary of dendrite complexity measured by Sholl analysis. Concentric spheres were centred on the cell body, and the radii were incremented by 10 μm. The number of branching points within each sphere was plotted as dendrite complexity (i.e. the number of intersections). $^{**}P < 0.01$.

Table 1. Basic electrophysiological properties of Purkinje cells

	Membrane capacitance (pF)[a,d]	Resting membrane potential (mV)[a]	Input resistance (MΩ)[a,d]	Percentage of cells showing spontaneous action potentials[b,e]	Frequency of spontaneous action potentials (Hz)[c,e]
GFP alone	39.2 ± 24.3 ($n = 35$)	−58.3 ± 13.6 ($n = 35$)	379 ± 278 ($n = 35$)	80% (12 of 15 cells)	0.43 ± 1.00 ($n = 15$)
WT mKv3.3	40.1 ± 16.1 ($n = 17$)	−59.9 ± 8.24 ($n = 17$)	367 ± 181 ($n = 17$)	75% (6 of 8 cells)	0.25 ± 0.59 ($n = 8$)
R424H mutant	22.3 ± 6.9*† ($n = 28$)	−59.5 ± 7.4 ($n = 28$)	372 ± 169 ($n = 28$)	64% (9 of 14 cells)	0.12 ± 0.75 ($n = 14$)

Here and in Table 2, statistical analysis was conducted between cells expressing the R424H mutant and those expressing green fluorescent protein (GFP) alone or between cells expressing R424H mutant and those expressing wild-type (WT) mKv3.3. Data are given as the means ± SD, and n is the number of experiments. *$P < 0.001$ between GFP alone and R424H mutant. †$P < 0.001$ between WT mKv3.3 and R424H mutant. The statistical analysis indicated by superscript letters a, b and c was conducted using Student's unpaired t test, the χ^2 test and Mann–Whitney U test, respectively. [d]Membrane capacitance and input resistance were measured in voltage-clamp conditions. [e]Spontaneous action potentials were recorded at resting membrane potential for 300 s.

compared with PCs expressing GFP alone or those expressing WT subunits (Table 1; resting membrane potential, R424H *versus* GFP, $P = 0.533$; R424H *versus* WT, $P = 0.874$; and input resistance, R424H *versus* GFP, $P = 0.882$; R424H *versus* WT, $P = 0.913$; analyses by Student's unpaired t test). Spontaneous action potentials were also observed in some PCs in all groups (Table 1 and Supplemental Fig. S4*B* and *C*). The percentages of PCs generating spontaneous firing and the frequency of the firing were comparable among the three groups (Table 1).

Outward currents were recorded in Hepes-buffered ACSF containing TTX, $CdCl_2$, picrotoxin and DNQX (see Methods). Representative current traces recorded from GFP-, WT- and R424H mutant-expressing PCs are illustrated in Fig. 4*A*. Depolarizing voltage pulses (more positive than −10 mV) evoked outward currents with a transient peak in GFP-, WT- and R424H mutant-expressing PCs (Fig. 4*A*). In WT-expressing PCs, peak amplitudes of the transient currents were larger than those in GFP-expressing PCs, indicating that lentivirally expressed mKv3.3 formed functional channels (Fig. 4*Ab*). In contrast, the peak amplitudes in R424H mutant-expressing PCs were smaller than those in GFP-expressing PCs (Fig. 4*Aa* and *Ac*). As the membrane capacitance of R424H mutant-expressing PCs was significantly smaller than that of GFP- and WT-expressing PCs (Table 1), the peak current amplitudes at voltages between +10 and +40 mV were normalized to membrane capacitances (current densities, in pico-amperes per picofarad; Fig. 4*B*). The current densities in R424H mutant-expressing PCs were ~2-fold smaller than those in GFP-expressing PCs at voltages between +10 and +40 mV (Fig. 4*B*), confirming that the expression of the R424H mutant subunits in cultured PCs suppressed outward currents in a dominant-negative manner.

Expression of R424H mutant subunits reduces sEPSCs in PCs

In standard culture conditions, PCs receive excitatory synaptic inputs from granule cells via the dendrites (Hirano *et al.* 1986; Hirano & Kasono, 1993). In order to examine how R424H mutant-induced impairment of dendritic development affects the synaptic inputs to PCs, sEPSCs were recorded from PCs in the presence of picrotoxin at a holding potential of −80 mV (Fig. 5). Examples of sEPSCs in GFP- or WT-expressing PCs appear as downward deflections in the current traces (Fig. 5*Aa* and *Ba*). These currents were abolished by application of 20 μM DNQX (traces not shown) and were thus identified as being mediated by AMPA/kainate receptors. Ensemble averages of the events in individual cells are also shown in Fig. 5*Ab* and *Bb*. Although sEPSCs in both groups were observed in all cells tested (Table 2), most R424H mutant-expressing PCs (10 of 13 cells) did not show sEPSCs during the 250 s recording period (Fig. 5*C* and Table 2; R424H and GFP, $P < 0.001$; R424H and WT, $P < 0.001$ by Fisher's exact probability test). Even in PCs showing sEPSCs, the frequency was significantly lower than in GFP- or WT-expressing PCs (Table 2). The R424H mutant-expressing PCs might receive few, if any, excitatory synaptic contacts onto their somata and dendrites.

R424H mutant-expressing PCs exhibit broadened action potentials and altered firing patterns

Expression of R424H mutant subunits in PCs suppressed outward current density, suggesting the alteration of the action potential waveform and firing properties in R424H mutant-expressing PCs. To examine these possibilities,

single action potentials (Fig. 6) and repetitive firings (Fig. 7) were evoked in current-clamp conditions. When a single action potential was evoked by short current injection (10 ms duration), R424H mutant-expressing PCs showed a broadened action potential waveform (Fig. 6*A*). The half-amplitude widths of R424H mutant-expressing PCs were 1.7-fold larger than those of GFP-expressing PCs (Fig. 6*B*; $P < 0.001$). The maximal rate of rise and maximal rate of fall in R424H mutant-expressing PCs were 0.75- and 0.65-fold of those in GFP-expressing PCs, respectively (Fig. 6*C* and *D*; maximal rate of rise, $P < 0.001$; maximal rate of fall, $P < 0.001$). These changes suggest that not only outward K^+ current but also voltage-dependent Na^+ current (I_{Na}) was affected by the expression of R424H mutant, because the maximal rate of rise of the action potential has been used as an index of the inward I_{Na} (Hodgkin & Katz, 1949).

To clarify the reduction of the maximal rate of rise by R424H mutant expression, I_{Na} was recorded from PCs in voltage-clamp conditions (Supplemental Fig. S5). Expression of R424H mutant subunits significantly reduced I_{Na} compared with the control group, without any changes in the voltage dependence of activation and inactivation. As the I_{Na} of cultured PCs is distributed through the cell body and axons (Fry *et al.* 2007), the reduction in I_{Na} would be due to the smaller cell body (Table 1, 'Membrane capacitance') and impaired neurite extension of R424H-expressing PCs. The expression of R424H mutant subunits did not affect the threshold current, threshold potential or action potential amplitude of PCs compared with expression of GFP (Fig. 6*E–G*). These results strongly suggest that expression of R424H mutant subunits inhibited the activation of the endogenous mKv3.3 channels, resulting in a reduction of the maximal rate of fall and then in the broadening of action potential duration in PCs.

We next examined the firing properties evoked by long current injection (200 ms duration). Most GFP-expressing PCs (82.9%) showed tonic firing of action potentials (tonic type) in response to depolarizing current injection (Fig. 7*A* and filled column of GFP in Fig. 7*E*), which is consistent with previous reports on the firing pattern of cultured PCs (Tabata *et al.* 2000; Harada *et al.* 2006). The other PCs (17.1%) showed a few spikes (up to three spikes) in response to current injection ranging from 0 to 200 pA

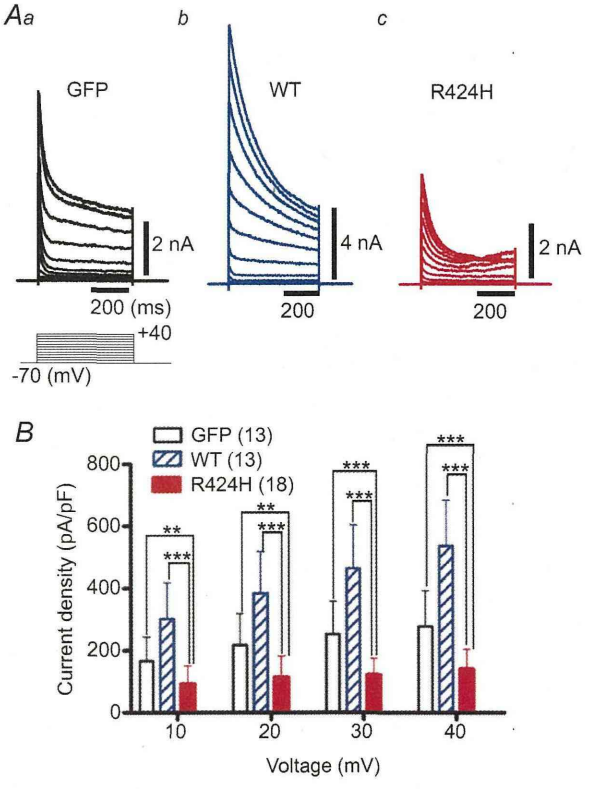

Figure 4. R424H mutant-expressing PCs exhibit suppressed peak outward current density
A, representative outward current traces recorded from PCs expressing GFP alone (*Aa*), WT subunits (*Ab*; note the vertical scale bar) and R424H mutant subunits (*Ac*). The currents were evoked by voltage steps from the −70 mV holding potential to voltages ranging from −60 to +40 mV in 10 mV increments. Leak currents were subtracted online by the *P*/4 protocol. The currents were recorded at DIV 8–10 in Hepes-buffered srtificial cerebrospinal fluid (ACSF) containing TTX, $CdCl_2$, picrotoxin and 6,7-dinitroquinoxaline-2,3-dione (DNQX). *B*, summary of the peak outward current density, which was calculated by dividing the peak outward current by membrane capacitance. $^{**}P < 0.01$ and $^{***}P < 0.001$.

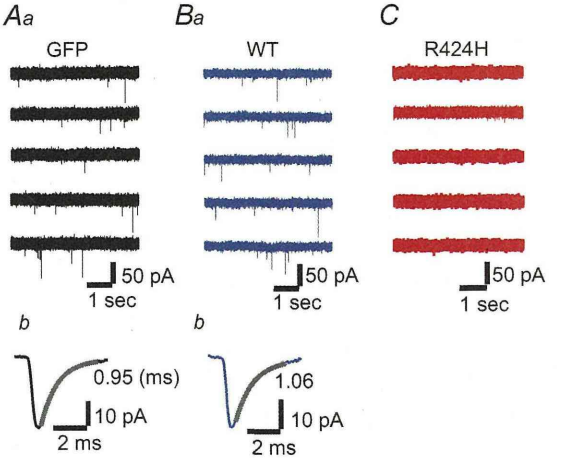

Figure 5. Absence of spontaneous excitatory postsynaptic currents (sEPSCs) in R424H mutant-expressing PCs
Aa, *Ba* and *C*, representative current traces recorded from PCs expressing GFP alone (*Aa*), WT subunits (*Ba*) or R424H mutant subunits (*C*). The sEPSCs appear as downward deflections in *Aa* and *Ba*. The PCs were held at −80 mV in the presence of picrotoxin. *Ab* and *Bb*, averaged sEPSCs from the same cell as in *Aa* and *Ba*, with superimposed single exponential fit. The decay time constant is indicated beside each trace.

Table 2. Summary of spontaneous excitatory postsynaptic current (sEPSC) properties in Purkinje cells

	Percentage of cells showing sEPSCs[a]	Amplitude (pA)[b]	Frequency (Hz)[b]	10–90% Rise time (ms)[b]	Decay time constant (ms)[c]
GFP alone	100%	33.7 ± 9.3	0.62 ± 0.35	0.18 ± 0.04	0.84 ± 0.27
(n = 15; 1502 events)	(15 of 15 cells)	(n = 15)	(n = 15)	(n = 15)	(n = 15)
WT mKv3.3	100%	34.0 ± 12.0	0.73 ± 0.35	0.19 ± 0.03	0.87 ± 0.19
(n = 10; 1041 events)	(10 of 10 cells)	(n = 10)	(n = 10)	(n = 10)	(n = 10)
R424H mutant	23%	23.1 ± 4.2	0.15 ± 0.10	0.20 ± 0.02	1.14 ± 0.21
(n = 3; 103 events)	(3 of 13 cells)**††	(n = 3)	(n = 3)*†	(n = 3)	(n = 3)

All measurements were performed at a holding potential of −80 mV. The statistical analyses indicated by superscript letters a and b were conducted using Student's unpaired t test and Fisher's exact probability test, respectively. [c]The sEPSC decay phases were fitted with a single exponential function. *P < 0.05, **P < 0.001 between GFP alone and R424H mutant. †P < 0.05, ††P < 0.001 between WT mKv3.3 and R424H mutant.

in 20 pA increments and did not fire tonically during the 200 ms depolarizing pulses (onset type; open column of GFP in Fig. 7*E*). However, approximately half of the R424H mutant-expressing PCs exhibited onset-type firing (53.6%; Fig. 7*C* and *E*), and the remaining PCs exhibited tonic-type firing (46.4%; Fig. 7*D* and *E*). The percentages of firing types in R424H mutant-expressing PCs differed significantly from those in GFP- and WT-expressing PCs (Fig. 7*E*; $P < 0.001$ in both pairs by the χ^2 test). The firing frequencies of tonic-type neurons in the three groups were plotted against the injected current (Fig. 7*F*). Wild-type-expressing PCs showed the highest frequencies, in the range of 40–200 pA (Fig. 7*B* and *F*), demonstrating that lentivirally expressed WT subunits contributed to the generation of narrow action potentials by accelerating the falling phase (Fig. 7*A* and *D* and Supplemental Fig. S3*E*). In tonic-type neurons, firing frequencies in R424H mutant-expressing PCs were significantly lower than those in GFP-expressing PCs, in the range of 180–200 pA (Fig. 7*F*; $P < 0.05$ at 180 and 200 pA depolarization). These results demonstrate that expression of R424H mutant subunits changed the ratio of tonic-firing PCs and reduced PC excitability in response to depolarization.

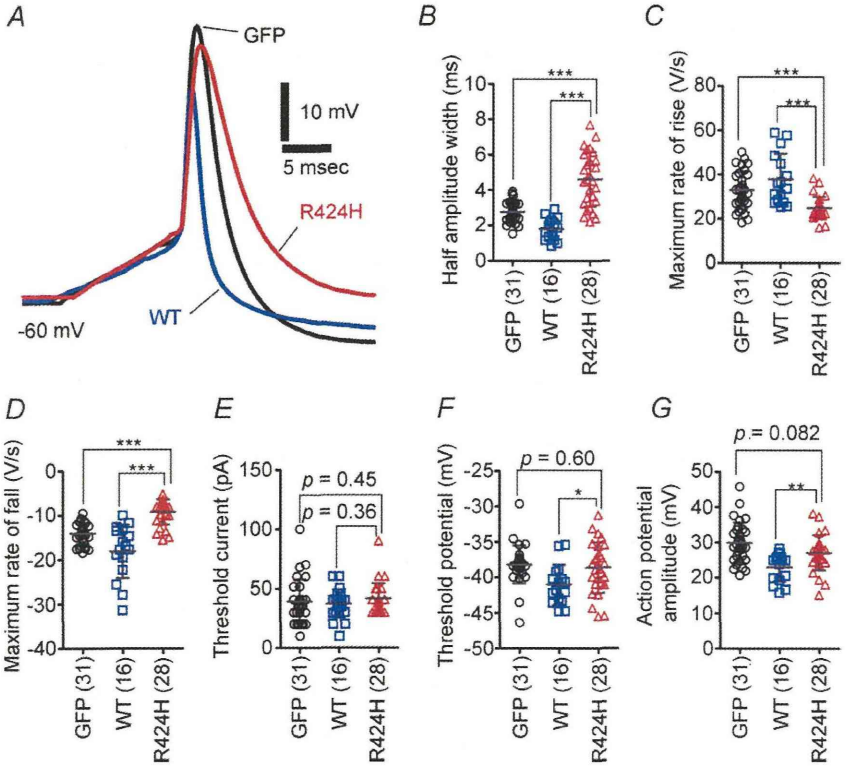

Figure 6. R424H mutant-expressing PCs exhibit broadened action potential waveforms
A, representative single action potential waveforms of PCs. The action potentials were evoked by short depolarizing current injection (10 ms duration). Action potentials were aligned by superimposing the rising phase of each trace. The resting membrane potentials were adjusted to −60 mV by current injection. *B*–*G*, comparison of action potential properties. *B*, half-amplitude width measured at the mid-point between the threshold and peak of the action potential. *C* and *D*, maximal rate of rise (*C*) and of fall (*D*) of action potentials. *E*, threshold current amplitude. *F*, threshold potential. *G*, action potential amplitude, as measured between the threshold and peak. *P < 0.05, **P < 0.01 and ***P < 0.001.

R424H mutant-expressing PCs show higher $[Ca^{2+}]_i$, and blockade of P/Q-type Ca^{2+} channels rescues the PC death and dendritic maldevelopment caused by the mutant subunits

The expression of R424H mutant subunits in cerebellar cultures caused PC death. We hypothesized that the cell death was caused by excessive Ca^{2+} influx through the following steps. As cultured PCs spontaneously generate action potentials, which increase basal $[Ca^{2+}]_i$ (Schilling *et al.* 1991; Supplemental Fig. S4*B* and *C* and Table 1), the broadening of action potentials by R424H mutant expression would cause increased Ca^{2+} influx via excessive activation of voltage-gated Ca^{2+} channels. This influx would lead to a defect of Ca^{2+} homeostasis in PCs, resulting in the cell death as a part of a stress response (Orrenius *et al.* 2003). Indeed, excessive Ca^{2+} influx triggered by the blockade of K^+ channels has been shown to induce cell death in several types of cells (Kim *et al.* 2000; Lajdova *et al.* 2004; Wang *et al.* 2011). To test this hypothesis, we performed calcium imaging (Fig. 8) and then rescue experiments of PC death using ω-agatoxin IVA, a specific blocker for the P/Q-type voltage-gated Ca^{2+} channels that mediate predominant Ca^{2+} currents in PCs (Mintz & Bean, 1993; Gillard *et al.* 1997; Fig. 9).

Calcium imaging was performed using cerebellar cultures loaded with fura-2 AM (see Methods). After a baseline recording (measurement of basal $[Ca^{2+}]_i$) for 8 min, cerebellar cultures were depolarized for 5 min by perfusion of high-K^+ ACSF (Fig. 8*B*). In basal conditions, $[Ca^{2+}]_i$ in R424H mutant-expressing PCs was approximately four times higher than in the control group (Fig. 8*Ca*; $P < 0.001$ in R424H *versus* GFP and in R424H *versus* WT). There were no significant differences in high-K^+-induced $[Ca^{2+}]_i$ elevation (~200 nM) between PCs expressing the R424H mutant and those expressing GFP alone or expressing WT subunits (Fig. 8*Cb*). The basal $[Ca^{2+}]_i$ of granule cells infected with the

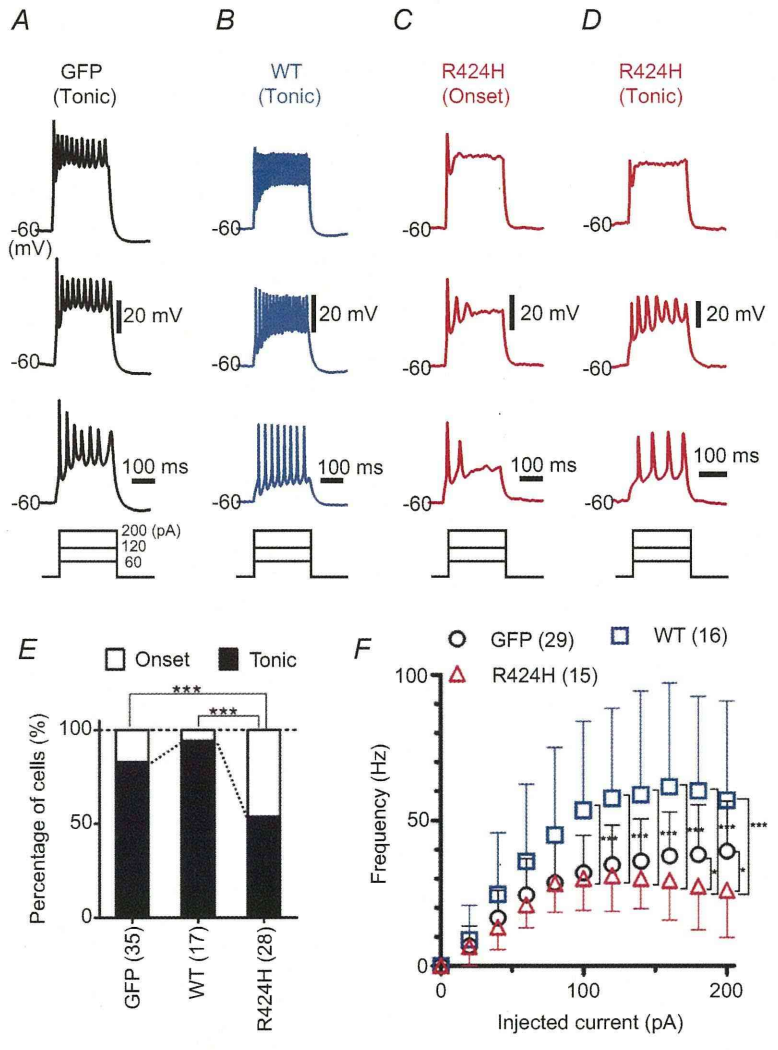

Figure 7. R424H mutant-expressing PCs exhibit altered firing patterns
A–D, representative firing patterns of PCs expressing GFP alone (*A*), WT subunits (*B*) or R424H mutant subunits (*C* and *D*). Approximately half of the R424H mutant-expressing PCs fired at the onset of current injection (onset-type; *C*). The action potentials were evoked by long depolarizing current injection (200 ms duration). The resting membrane potentials were adjusted to −60 mV. *E*, comparison of firing patterns. The χ^2 test was used for the statistical analyses. *F*, the firing frequency of the tonic-type cells is plotted as a function of injected current. $^*P < 0.05$ and $^{***}P < 0.001$.